# Characterization of carboxylate nanoparticle adhesion with the fungal pathogen *Candida albicans*

Amy Lyden,[a] Lisa Lombardi,[b] Wilfried Sire,[c] Peng Li,[a] Jeremy C. Simpson,[d] Geraldine Butler, [b] and Gil U. Lee [a]

*Candida albicans* is the lead fungal pathogen of nosocomial bloodstream infections worldwide and has mortality rates of 43%. Nanoparticles have been identified as a means to improve medical outcomes for *Candida* infections, enabling sample concentration, serving as contrast agents for *in vivo* imaging, and delivering therapeutics. However, little is known about how nanoparticles interact with the fungal cell wall. In this report we used laser scanning confocal microscopy to examine the interaction of fluorescent polystyrene nanoparticles of specific surface chemistry and diameter with *C. albicans* and mutant strains deficient in various *C. albicans* surface proteins. Carboxylate-functionalized nanoparticles adsorbed mainly to the hyphae of wild-type *C. albicans.* The dissociative binding constant of the nanoparticles was ~150, ~30 and ~2.5 pM for 40, 100 nm and 200 nm diameter particles, respectively. A significant reduction in particle binding was observed with a Δals3 strain compared to wild-type strains, identifying the Als3 adhesin as the main mediator of this nanoparticle adhesion. In the absence of Als3, nanoparticles bound to germ tubes and yeast cells in a pattern resembling the localization of Als1, indicating Als1 also plays a role. Nanoparticle surface charge was shown to influence binding –positively charged amine-functionalized nanoparticles failed to bind to the hyphal cell wall. Binding of carboxylate-functionalized nanoparticles was observed in the presence of serum, though interactions were reduced. These observations show that Als3 and Als1 are important targets for nanoparticle-mediated diagnostics and therapeutics, and provide direction for optimal diameter and surface characteristics of nanoparticles that bind to the fungal cell wall.

## Introduction

Candidiasis is considered the most critical life-threatening fungal infection for hospital patients worldwide and the fourth most common health-care associated bloodstream infection.[1,2] Despite its association with increased healthcare costs and fatalities, incident rates and associated mortality have not improved in the last two decades. [1,2] *Candida albicans* is the most common fungal cause of nosocomial bloodstream infections in most countries, causing approximately 50% of all cases of candidiasis and having overall mortality rates of 43%. [2,3] This commensal organism is found in oral, digestive and reproductive cavities of the human body, but can cause systemic infections under certain conditions, especially in immunocompromised patients.[4] Pathogenic yeast can adhere to surfaces like tissue and medical devices, and form biofilms, complex yeast communities that are often resistant to antimicrobials and are a source of persistent infections.[4]

Rapid and inexpensive diagnosis to avoid treatment delay and effective antifungal treatment of biofilms are two unmet needs in the treatment of fungal bloodstream infections. The first, rapid and inexpensive diagnosis of fungal bloodstream infections, is crucial to prevention of fatalities. Many patients displaying signs of infection are mistakenly placed on antibiotics, and thus there is a need to specifically distinguish between bacterial and fungal infections.[1] The main method of diagnosis is a blood culture, which can take 1-7 days for positive results and has specificity of only 50%.[2] Other developing non-culture methods include real time polymerase chain reaction (PCR), matrix-assisted laser desorption/ionization time-of-flight mass spectrometry, and nanoparticle capture of molecular targets in blood samples combined with T2 magnetic resonance, all of which require significant sample preparation and/or expensive lab equipment.[5–7] Thus, they have not yet been widely adopted. Additionally, these all occur *in vitro*: an *in vivo* diagnostic could provide more information about location and stage of infection, as well as be combined with a therapeutic. The second unmet need, treatment of biofilms, poses a unique challenge – biofilm attachment is associated with pathogenicity and increased antimicrobial resistance, and they can form rapidly in 48 hours.[4,8] *C. albicans* biofilms in particular have been shown to be display resistance mechanisms such as the presence of persister cells.[8] Novel therapeutics against pathogenic yeast and fungal biofilms are urgently needed.

Nanoparticles have emerged as powerful new enablers for therapeutic and diagnostic agents. Nanoparticles can be functionalized with ligands to promote targeting of cells and tissues, and drugs can be adsorbed or conjugated onto the surface or encapsulated within the interior of nanoparticles for specific delivery. This allows controlled and localized release of a drug, and has shown promise in targeting bacterial infections with antibiotics. Superparamagnetic nanoparticles also have the potential to provide an economical, faster sample preparation for the capture of *C. albicans* for PCR[5] or magnetic

[a] School of Chemistry, University College Dublin, Belfield, Dublin 4, Ireland. Email: amy.m.lyden@gmail.com, gil.lee@ucd.ie
[b] Conway Institute, School of Biomolecular and Biomedical Science, University College Dublin, Belfield, Dublin 4, Ireland.
[c] Grenoble-INP Phelma, 3 Parvis Louis Néel, 38000 Grenoble, France
[d] School of Biology & Environmental Science, University College Dublin, Belfield, Dublin 4, Ireland.

resonance assays[7], and serve as contrast agents for *in vivo* imaging for detection and localization of fungal infections.[9]

Despite the potential for nanoparticles in diagnosis and treatment of fungal bloodstream infections, limited information is available to guide the design, particularly in relation to physiochemical properties of nanoparticles such as surface charge and size. Surface charge governs electrostatic interactions between the cell wall and nanoparticle. Both size and surface charge influence whether a particle adsorbs or is taken up by a cell.[10] Additionally, the formation of a protein layer surrounding the exterior of the nanoparticle can influence interactions *in vivo*.[11] Characterization of these interactions based on physiochemical properties will facilitate the effective design of nanoparticles for targeting *C. albicans*.

Bacterial cell wall interactions with nanoparticles of different shape, diameter and surface charge have been studied previously, and it has been found that these nanoparticle characteristics affect interaction and toxicity.[12–14] For example, positively charged gold nanoparticles show high levels of toxicity against *Escherichia coli* whereas anionic gold nanoparticles are nontoxic, due to the negatively charged lipid membrane of *E. coli.*[15] These results suggest that nanoparticle properties influence interactions with pathogens, but yeast specific studies are still needed. Though bacteria and yeast share some common pathogenic traits, such as biofilm formation, they present distinct properties. Yeast cells are larger than bacterial cells and have different cell wall compositions. [16,17] Additionally, yeast infections pose particularly unique challenges, as certain species, including *C. albicans*, create more uniform and cohesive biofilms with the formation of filaments, or hyphae, than bacterial biofilms.[18] Nanoparticles can tackle the more complex fungal biofilm. Silver nanoparticles have been shown to damage *C. albicans* cell wall.[19] Magnetic nanoparticles bound to antifungals in particular have shown promise in inhibiting biofilm growth.[20,21] However, basic studies on yeast cell wall interactions with nanoparticles of varying physiochemical properties must be performed to guide future research.

*C. albicans* exists in several growth states, including yeast, pseudohyphae and hyphae.[22] Switching from yeast to hyphal growth is associated with virulence.[16] Yeast cells attach to a surface and form a biofilm, a complex community of predominantly hyphal cells with a thick extracellular polymeric matrix.[16,18] In each state, the *C. albicans* cell wall displays different surface proteins[23], which alter their surface chemistry, including cell surface hydrophobicity[24] and surface charge. This has the potential to allow us to detect and treat *C. albicans* at its various stages of development, as free-living cells and in biofilms. Here, we studied the interaction of nanoparticles with *C. albicans* yeast and hyphae. We identified hyphal surface proteins required for adhesion to carboxylate-functionalized nanoparticles and we characterized the physiochemical properties of nanoparticles that affect nanoparticle adhesion.

## Experimental

**Polystyrene nanoparticles**

Polystyrene nanoparticles were obtained from Thermo-Fisher Invitrogen, Molecular Probes. We used red fluorescent (580/605 nm) FluoSpheres Carboxylate-Modified Microspheres with diameters of 40 nm, 100 nm and 200 nm and red fluorescent (580/605 nm) FluoSpheres Amine-Modified Microspheres with diameter of 200nm. Particles were diluted in Dulbecco A phosphate buffered saline (Thermo Fisher Scientific, Oxoid Microbiology; sodium chloride 8g/L, potassium chloride 0.2 g/L, disodium hydrogen phosphate 1.15 g/L, potassium dihydrogen phosphate 0.2 g.L, pH 7.3), vortexed for 30 seconds and sonicated for at least 1 minute after dilution to minimise aggregation.

**Characterization of Nanoparticles**

Dynamic light scattering and electrophoretic light scattering (Malvern Instruments Zetasizer Nano Series) were used to characterize the particle diameter, dispersity and zeta potential. Samples were diluted to 100 µg/mL in distilled water, Dulbecco A phosphate buffered saline (PBS) or fetal bovine serum (FBS, Sigma Aldrich Life Science) in PBS. Table 1 summarized the nanoparticle properties as a function of particle physical properties and aqueous media. Carboxylate nanoparticle stability was also evaluated during a pH titration; results can be found in Supplementary Information Table S1. Hydrodynamic diameter and zeta potential were found to be in agreement with previously reported literature[25,26] and in

**Table 1.** DLS Characterization of polystyrene nanoparticles used in this study in various medium [1]Each zeta potential (ZP) is an average of three independent measurements, each three measurements of 20 runs each. [2]Each hydrodynamic diameter (HD) is an average of three independent measurements, each three measurements of 11 runs each. [3]Each polydispersity index (PDI) is an average of three independent measurements, each three measurements of 11 runs each.

| Surface Group | Nominal Diameter (nm) | Media | ZP[1] (mV) | HD[2] (nm) | PDI[3] |
|---|---|---|---|---|---|
| Carboxylate | 200 | Distilled Water | -64.9.3±8.4 | 214.1±4.7 | 0.01±0.01 |
| Carboxylate | 100 | Distilled Water | -55.8±0.8 | 133.0±1.8 | 0.02±0.01 |
| Carboxylate | 40 | Distilled Water | -56.2±7.2 | 59.6±1.2 | 0.10±0.03 |
| Carboxylate | 200 | PBS | -35.4±1.6 | 208.2±5.5 | 0.02±0.01 |
| Carboxylate | 100 | PBS | -31.5±2.8 | 131.9±2.1 | 0.04±0.02 |
| Carboxylate | 40 | PBS | -31.3±1.7 | 59.3±8.2 | 0.16±0.1 |
| Carboxylate | 200 | 10% FBS in PBS | -8.3±1.7 | 255.8±8.1 | 0.06±0.01 |
| Carboxylate | 40 | 5% FBS in PBS | -9.9±0.6 | 119.5±24.9 | 0.2±0.01 |
| Carboxylate | 40 | 10% FBS in PBS | -8.9±1.0 | 130.1±30.3 | 0.23±0.01 |
| Carboxylate | 40 | 20% FBS in PBS | -7.0±0.5 | 90.9±13.2 | 0.28±0.01 |
| Amine | 200 | Distilled Water | 43.1±3.6 | 553.8±111.5 | 0.28±0.01 |
| Amine | 200 | PBS | 10.0±0.8 | 621.4±42.3 | 0.34±0.03 |

reasonable concurrence with nominal diameter as listed by manufacturer. TEM images of particles confirm they are uniform in diameter and in concurrence with nominal diameter (Supplementary Information Figure S1). Polydispersity index (PDI) indicated reasonably monodispersed homogenous particle distribution in distilled water and PBS, though higher PDI values for carboxylate nanoparticles in FBS and amine particles in water and PBS indicate particle interaction takes place.

### *C. albicans* strains and media

All *C. albicans* strains were obtained from Professor Lois Hoyer and Aaron Mitchell and are listed in Table 2. Details of construction can be found in references. All isolates were stored at -80°C in yeast-peptone-dextrose medium (ForMedium, 2% Bacto peptone, 2% glucose, 1% yeast extract) supplemented with 15% of glycerol (Sigma Life Science, ≥99%). Colonies were formed by streaking onto yeast-peptone-dextrose (YPD) agar plates (YPD + 1.5% agar). Yeast form was obtained after growth in YPD medium. Germ tube growth was performed in 1.04% RPMI 1640 (RPMI 1640 with L-glutamine from Sigma Life Science) in 3.75% MOPS (4-Morpholinepropanesulfonic acid from Sigma Life Science ≥99.5%). Hyphal growth was performed in Spider medium (1% nutrient broth from Fluka Analytical Sigma Aldrich, 1% mannitol from Sigma Aldrich >98%, 0.2% potassium phosphate from Fluka Chemie Sigma Aldrich >99%).

### *C. albicans* culture conditions

Strains were streaked onto YPD agar plates and grown at 30°C for 36-48 h. Plates were stored at 4°C for up to 2 weeks and then streaked again. A single colony was used to inoculate an overnight (ON) culture in 5 mL of YPD medium. The culture was placed on a shaker at 200 rpm at 37°C and grown for 16 h. One mL from the ON culture was washed twice in PBS. Cultures were diluted to an optical density of 1 at 600 nm ($A_{600}$) in PBS, which equates to approximately 20 x $10^6$ cells/mL. Cells were spun down at 17000 rcf for 1 min and suspended in the appropriate medium to induce germ tube and hyphal development.

### Germ tube and hyphal development

Experimental conditions for germ tube growth match those followed by Hoyer et al (2014)[27]. 4 x $10^6$ cells were suspended in 200 µL pre-warmed RPMI 1640, pH 7 for final $A_{600}$ of 1 and incubated at 37°C for 90 min in a stationary 1.5 mL microfuge tube. After incubation, cells were spun down at 17000 RCF for 3 min, washed once in PBS and then suspended in PBS at the same concentration. 5 µL of 0.2 mM Calcofluor White (CFW, 0.2 mM Fluorescent Brightener 28, Sigma Life Science) was added to stain the chitin in the yeast cell wall. 20µL of polystyrene nanoparticles diluted in PBS were added at this point, for a final nanoparticle concentration of 20µg/mL (or as otherwise indicated). Samples were vortexed for 30s and placed on a rotator at 4°C overnight. Germ tubes were examined for morphology and length to distinguish from pseudohyphae based on guidelines outlined by Sudbery et al (2004)[22] and Zhao et al (2004)[28] and had to match the following criteria:

1. Germ tube length equivalent or longer than the diameter of the mother yeast cell
2. Completely parallel cell walls
3. No visible constriction in cell wall at neck or septum
4. No septum at mother-bud neck as visible with CFW staining

Hyphae were induced by incubating 4 x $10^6$ cells in 200 µL for final $A_{600}$ of 1 at 37°C for 3 or 6 hours in Spider media at pH 7.2 in a stationary 1.5 mL microfuge tube. 5 µL of 0.2 mM CFW was added for 10 min. After incubation, cells were spun down at 17000 RCF for 3 min, washed once in PBS and then suspended in 200 µL PBS. FBS was added where indicated. 5 µL of polystyrene nanoparticles diluted in PBS at the appropriate concentration were added to the sample. Samples were vortexed for 30s and placed on a rotator at 4°C overnight.

**Table 2. *C. albicans* strains: Relevant information about the strains used in this study.** All the mutant strains used were derived from the wild-type strain SC5314. Details of strain construction can be found in references. Analysis of growth rates of strains can be found in Supplementary Information Table S2.

| Strain | Designation | Genotype | Parental strain | Reference |
|---|---|---|---|---|
| SC5314 | Wild-type | *URA3/URA3 ARG4/ARG4 HIS1/HIS1* | – | Gillum et al. (1984)[29] |
| CAI12 | CAI12 | *iro1-Δura3::imm434/IROI URA3* | CAI4 | Porta et al. (1999)[30] |
| 1467 | Δals1 | *ura3/ura3 als1/als1-URA3* | CAI4 | Zhao et al. (2004)[28] |
| 2757 | Δals2 | *ura3/ura3 als2/als2-URA3* | CAI4 | Harriott & Noverr (2010)[31] |
| 1843 | Δals3 | *ura3/ura3 als3/als3-URA3* | CAI4 | Zhao et al. (2004)[28] |
| 2034 | Δals4 | *ura3/ura3 als4/als4-URA3* | CAI4 | Zhao et al. (2005)[32] |
| CAI4-URA3 | CAI4-URA3 | *ura3 :: imm434/ura3 :: imm434 pARG4-URA3* | CAI4 | Sanchez et al. (2004)[33] |
| CAH7-1A1E2 | Δhwp1 | *ura3 :: imm434/ura3 :: imm434 hwp1::hisG/hwp1::hisG eno1::URA3/ ENO1* | CAI4 | Sundstrum et al. (2002)[34] |

### Microscopy

Epifluorescence microscope images were taken with an Olympus IX73 using a 100x/1.30NA UPlanFL oil immersion objective with Hamamatsu ORCA-Flash 4.0 camera using CellSens Dimension 1.9 software. Confocal microscope images were taken on Olympus Fluoview FV1000 using a 60x/1.35NA UPlanSApo oil immersion objective. CFW staining and red fluorescent nanoparticles were imaged using 405 nm and 559nm laser line, respectively and sequential imaging was used. Exposure, power, zoom, offset, and gain were all fixed within an experimental data set. For all but z-stacks, sampling speed was 10 µs/pixel and a line Kalman filter of 4 was applied. For confocal stacks, sampling speed was 12.5 µs/pixel and a line Kalman filter of 3 was applied.

### Image Analysis

Images were compiled and analyzed in ImageJ (National Institutes of Health). Integrated density measurements of nanoparticle fluorescence intensity were taken along hyphae using a one micron square parallel to the hyphal wall. For each image, five background measurements were taken and the average subtracted from the intensity value. For 200 nm nanoparticles, the fluorescent intensity of 10 monomers was measured and averaged. The standard deviation of intensity of a monomer was found to be less than 10% of the total intensity. The total intensity along the hyphae was divided by the average intensity of the 200 nm nanoparticle. Z-stacks were analyzed with deconvolution software and cross-sections were displayed in Imaris.

### Statistical analysis

All P-values given are Welch unpaired two-sided t-tests of unequal variances, unless stated as a one-sided t-test or a one-way ANOVA. Statistics were evaluated using RStudio 0.99.491, with R 3.2.3.

## Results and Discussion

In this study we characterized nanoparticle interaction with *C. albicans* with high resolution epifluorescence and confocal microscopy. This allowed us to identify the location of nanoparticle attachment at various growth phases of *C. albicans*. These results demonstrate that that nanoparticle surface charge and diameter, as well as the presence of serum, affected nanoparticle adhesion with *C. albicans*. Using strains deficient in the production of certain surface proteins, we identified the proteins mediating carboxylate nanoparticle adhesion.

### Nanoparticle attachment to wild-type yeast

Figure 1A presents a schematic of *C. albicans* morphology at various growth phases, key to understanding nanoparticle attachment to *C. albicans*. For hyphae to develop, short germ tubes (2 microns in width) bud from yeast cells (rounded cells approximately 5-10 microns in diameter) and develop into longer, filamentous hyphae with septum. Pseudohyphae (greater than 2.8 micron in width) also form from yeast and are a distinct state from hyphae, despite their elongated appearance. Virulence and biofilm formation is associated with hyphal growth[16,18] which is induced under physiological conditions such as growth at 37°C, pH 7 and in the presence of serum.[16] Many other conditions are known to induce hyphal development including growth in Spider media, RPMI 1640 and Lee's medium.[16,22] We chose a wild-type strain of *C. albicans,* SC5314[29] for initial studies of nanoparticle behaviour, and Spider media and RPMI 1640 were used to induce hyphal growth.

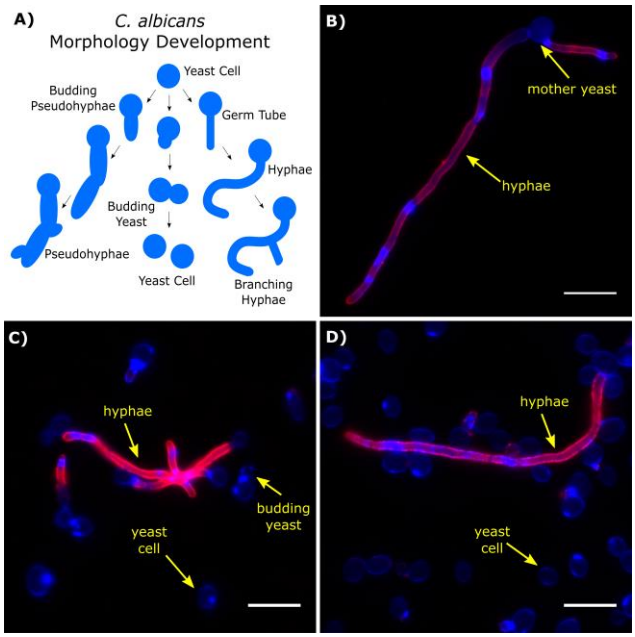


**Figure 1.** Adsorption of carboxylate polystyrene nanoparticles on *C. albicans.* **A:** Different morphology of *C. albicans* starting from yeast phase, and leading to pseudohyphae, daughter yeast, and hyphae (based on Sudbery et al 2004). **B-D:** Epifluorescence images of *C. albicans* SC5314 strain stained with 0.2 mM CFW (blue) after hyphal development in Spider media for 6 hours and reacted with carboxylate nanoparticles (red) with the indicated diameters and concentrations Listed below. Yeast and hyphal cells are labelled in yellow. **B.** 40 nm (5 µg/mL), **C.** 100 nm (10 µg/mL), **D.** 200 nm (10 µg/mL). All scale bars represent 10 µm in length.

In both Spider media and RPMI 1640, germ tubes were formed at 1.5 hours, hyphae ranging 10-50 microns in length were formed after 3 hours and longer hyphae and hyphal aggregates were observed at 6 hours. After 6 hours of culture at a seeding density of 19-23 x $10^6$ yeast cells, we consistently obtained a heterogeneous population of yeast, pseudohyphae and hyphae (Figure 1).

Figures 1B-D show epifluorescence images of carboxyl functionalized polystyrene nanoparticle (red regions) adsorbed on *C. albicans.* The chitin in the *C. albicans* cell wall is stained with calcofluor white (CFW) and appear blue in the images. The nanoparticles in this study are uniform in diameter and surface charge (Table 1, Supplementary Information Figure S1), and have been used previously with mammalian cells, bacterial cells and *Saccharomyces cerevisiae*[11,35,36]. We observed that the negatively charged nanoparticles bind predominantly to the hyphae of *C. albicans*, regardless of particle diameter. Nanoparticle fluorescence appeared along the entire length of the hyphae (Figure 1B-D). The resolution of these epifluorescent

images did not allow us to determine if nanoparticles were bound to the exterior of the hyphae, or uptaken within the cell, as has been shown with carboxylate nanoparticles in mammalian cells.[35] We therefore used confocal laser scanning microscope images and cross-sectional reconstructions of the carboxyl functionalized nanoparticle adsorbed on the CFW stained cell wall of *C. albicans* SC5314 (Figure 2). Because the red fluorescence intensity is proportional to number of beads, these high resolution images allow us to conclude that that the nanoparticles are located exclusively on the exterior of the hyphae and are not taken up by the cell. Both the 40 (Figure 2A) and 200 nm (Figure 2B) nanoparticles were characterized.

**Figure 2.** Confocal and reconstructed cross-sectional images of *C. albicans* SC5314 reacted with carboxylate nanoparticles (red) of indicated diameter and concentration. **A.** 40 nm (20µg/mL) **B.** 200 nm (20µg/mL). *C. albicans* was stained with 0.2 mM CFW (blue) after hyphal development in Spider Medium for 6 hrs. Side and bottom panels of each figure show z-stack cross sections (taken in 0.3 µm slices) of main center image across the yellow line. X, Y, and Z denote planes. Scale bars are 5 µm in length.

**Nanoparticle adsorption to *C. albicans* mutants**

Our observation that nanoparticles bind to the hyphae only implies that they interact with hyphal specific proteins. Potential candidates include members of the Als (Agglutinin-like sequence) family, a well-characterized set of proteins crucial for adhesion and aggregation of *C. albicans* to abiotic surfaces and host tissue[28,37–39] to yeast species such as *Candida glabrata*[40] and to bacteria including oral streptococci and *Staphylococcus aureus.*[27,41–43] Deletion of *ALS3* in particular has been shown to result in the greatest reduction in the adhesive properties of *C. albicans* in these interactions.[28,37,43] The Als3 protein is present on hyphae and not on yeast cells, and is required for mature-biofilm formation, binding extracellular matrix, adhesion to host cells, and internalization of *C. albicans* by endothelial cells (reviewed by Hoyer et al, 2016). Als1 has also been shown to function in adhesion to endothelial cells[28] and *C. glabrata.*[40] In addition to Als proteins, Hwp1, a hyphal specific protein, has been implicated in adhesion to human epithelial cells, and is essential for biofilm formation *in vivo*.[44,45] We therefore investigated the roles of four Als proteins (Als1, Als2, Als3, Als4) and of Hwp1.

Figure 3A shows confocal micrographs of 200 nm carboxylate nanoparticles binding to strains that are deficient in either Als or Hwp proteins (Materials and Methods, Table 2). All strains formed germ tubes and hyphae as previously reported.[28,32,34] Adherence of nanoparticles was observed using both epifluorescence (not shown) and confocal microscopy as shown in Figure 3A. Deleting *ALS1, ALS2, ALS4, or HWP1* had no effect on adherence of the nanoparticles, which showed the same pattern of binding as the two wild-type strains (SC5314 and CAI12). However, in the strain in which *ALS3* was deleted, the nanoparticles no longer bound to the hyphae that are generated (Figure 3A). We observed reduced nanoparticle binding along the entire length of the hyphae. We also observed some localized binding around the mother cell, at the junction of mother cell and the hyphae, and on some yeast cells (Figure 3A, Δals3, arrows).

To characterize the levels of nanoparticle binding in the mutant *C. albicans* strains, fluorescent intensity was measured at 10 random locations on the hyphae. The intensity was converted to the number of nanoparticles per micron of hyphae by normalising with the intensity of a single particle (Figure 3B). No statistically significant difference was observed between SC5314, Δals1, Δals2, Δals4, Δhwp1, CAI4-URA3 and CAI12 control strains ($P > 0.1$, one-way ANOVA). However, a highly significant reduction in binding was observed between Δals3 and both CAI12 and SC5314 ($P<0.0005$). These results are consistent with a model in which Als3 plays the primary role in the adhesion to negatively-charged nanoparticles, with little to no contributing effects from Als1, Als2, Als4 or Hwp1.

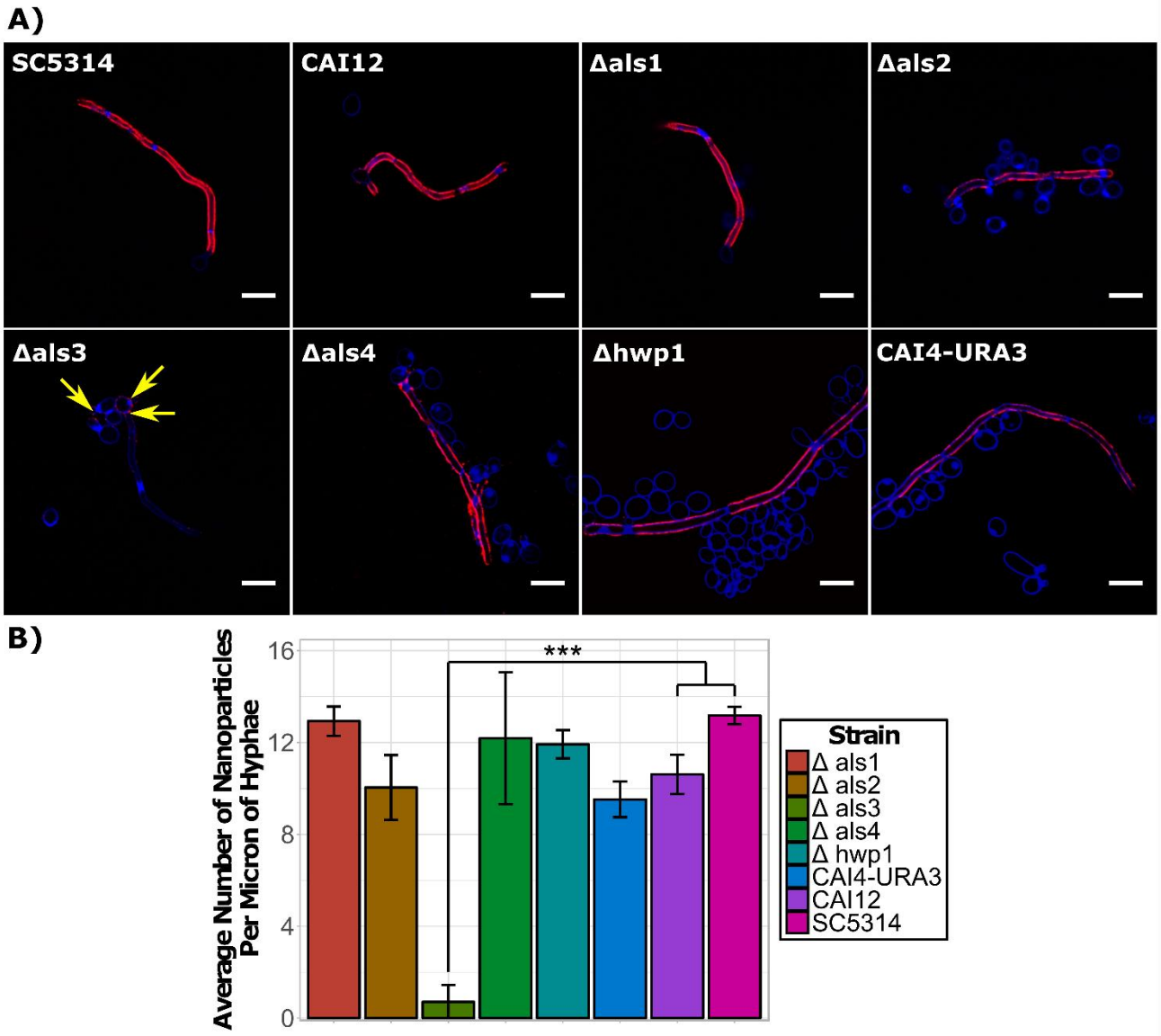


**Figure 3.** Confocal images and quantitative measurements of carboxylate nanoparticles adsorption on *C. albicans* mutant strains **A.** Confocal images of wild-type and Als mutant strains (Δ denotes deletion) stained with 0.2 mM CFW (blue) after hyphal development and reacted with 20 µg/mL of 200 nm red carboxylate nanoparticles (red). Scale bars represent 10 µm in length. **B.** Average number of 200 nm nanoparticles per micron of hyphae for *C. albicans* strains. For each cell, 10 measurements were taken along the hyphae and averaged. The data points and error bars represent the mean and standard deviation of at least 3 cells. (*** $P \leq 0.001$)

**Regional nanoparticle adherence**

Based on previous studies of the localization of Als proteins[46,47] we examined a population of germ tubes (RPMI 1640, pH 7 for 90 mins) and categorized them based on binding patterns. Figure 4A presents representative images of each category. Because we observed localization of nanoparticle binding around the neck in the Δals3 strain (Figure 3A, Δals3), we also categorized localization in a Δals1 deletion, because Als1 is known to be displayed on the neck of the germ tube.[46] As shown in Figure 4B, each category is distinct, i.e., separation of categorical means was significant within each strain ($P<0.005$, one-way ANOVA). There is no significant difference in the categories between the control strains (SC5314 and CAI12) and *Δals1* deletion strain ($P>0.05$). The deletion of *ALS3* greatly increased the percentage of cells with beads localized at the bud neck (Category 4, $P<0.005$, one-sided t-test) and with no bound beads (Category 7, $P<0.02$, one-sided t-test), and significantly reduced the percentage of cells with binding over the entire germ tube (Category 1, $P<0.005$, one-sided t-test). Only 4% of germ tubes in the Δals3 strains showed complete coverage by nanoparticles, compared to 50-55% observed in the other three strains.

Figure 4C presents the analysis of 100-150 yeast phase cells (RPMI 1640, pH 7 for 90 mins) that were categorized based on the amount of exterior surface area covered in nanoparticles. Cells were assigned to three categories: > 50% coverage (Yes), 1-50% coverage (Some) or <1% coverage (No). Only single

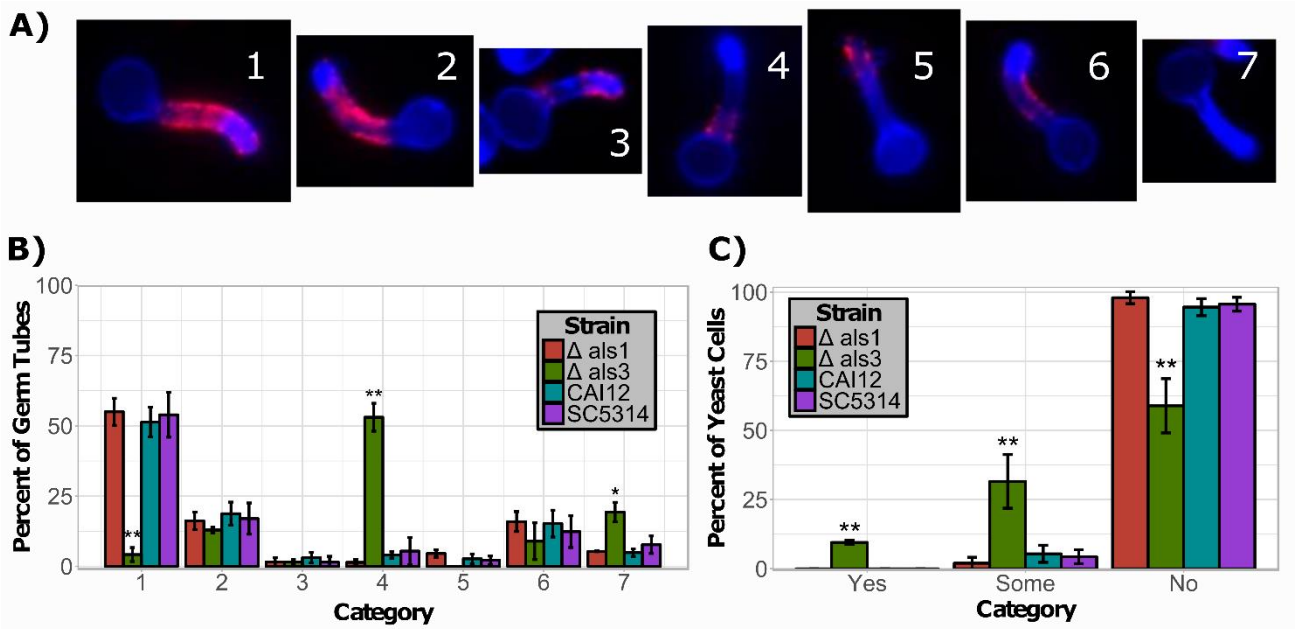


**Figure 4**. Classification of nanoparticle adsorption on *C. albicans* germ tubes and yeast phase cells. **A.** Representative images of germ tubes for categories studied. *1.* Complete coverage of germ tube (>50%) *2.* Complete area coverage of germ tube except for tip *3.* Localization at neck and tip *4.* Localization at neck only *5.* Localization at tip only *6.* Incomplete coverage without localization (<50%) *7.* No coverage **B.** Localization of carboxylate 200 nm nanoparticles on germ tubes grown in RPMI 1640, pH 7 for 90 minutes. For each biological replicate taken on a different day from a different culture, 90-110 germ tubes were counted. Bar height represents the mean of the three replicates and error bars show standard deviation. (* $P \leq 0.05$, ** $P \leq 0.01$). **C.** Coverage of yeast phase cells with carboxylate 200 nm nanoparticles, grown in RPMI 1640, pH 7 for 90 minutes. *1.* Yes (>50% area coverage) *2.* Some (1-50% area coverage) *3.* No (0% area coverage). For each biological replicate, 100-150 yeast cells were counted. Bar height represents the mean of the three replicates and error bars show standard deviation. (** $P \leq 0.01$)

yeast cells, with no daughter cells, aggregates or developing germ tubes, were counted. There is no binding to the majority of yeast cells (mean < 6%) in *C. albicans* CAI12, SC5314 and Δals1 strains, and the differences between these three strains was insignificant in all categories (P>0.4, one-way ANOVA). However, the Δals3 strain showed significant variation in all categories (P<0.005, one-way ANOVA). There was a statistically significant increase in cells that were mostly or partially coated with beads in the Δals3 strain when compared to both SC5314 and CAI12 (P<0.03, one-sided t-test). These results support our hypothesis that the hyphal specific interaction between *C. albicans* and the carboxylate nanoparticles is facilitated by Als3. With no Als3 available as a binding site, the nanoparticles are more likely to bind to yeast phase cells than in the wild-type strains.

### Influence of nanoparticle surface charge and diameter on adhesion

To quantify the effect of negative and positive surface charge on hyphal interactions, we measured the adsorption of 200 nm carboxylate and amine nanoparticles of opposite charge at varying concentrations to *C. albicans* SC5314 hyphae grown in Spider medium for 6 hours. We observed that the amine nanoparticles did not bind to the surface of the hyphae in the same manner as carboxylate nanoparticles (Figure 5A,B). Figure 5C presents the binding profiles confirming little to no binding of the positively charged nanoparticles. The adsorption of 200 nm amine nanoparticles compared to 200 nm carboxylate nanoparticles was reduced at all concentrations (P<0.05). The maximum number of nanoparticles per micron of hyphae, which occurs at 7.6 pM, was 14.2 ± 0.9 for the carboxylate nanoparticles and 0.7 ± 0.3 for the amine nanoparticles, illustrating that amine nanoparticles bound to the surface of the hyphae was significantly lower (P=0.000006) even under high concentration. It is important to note that in the medium studied (PBS), the zeta potential of amine particles is 11mV, while the carboxylate nanoparticles have a zeta potential of -33mV (Table 1). Thus, the charges are opposing but not equal in magnitude. The interaction between nanoparticles and the *C. albicans* surface is therefore highly dependent on the high negative charge surface of the nanoparticle. Additionally, because the amine nanoparticles displayed some interaction and aggregation in PBS (Table 1), extracting further quantitative information comparing the binding affinity of the nanoparticles would be unreasonable.

We examined three diameters of nanoparticles to compare size-dependent binding affinity for the hyphal cell wall. Using confocal microscopy images, the adsorption of 40 nm, 100 nm, and 200 nm nanoparticles on *C. albicans* SC5314 hyphae after 3 hours of growth in Spider medium was quantified at increasing nanoparticle concentrations, until a saturated

**Figure 5.** Influence of the nanoparticle physiochemical properties on adsorption to *C. albicans* hyphae. Confocal images of *C. albicans* SC5314 cells stained with 0.2 mM CFW after hyphal development and reacted with 40 ug/mL of 200 nm amine (**A**) vs carboxylate (**B**) red particles. All scale bars represent 10 µm in length.

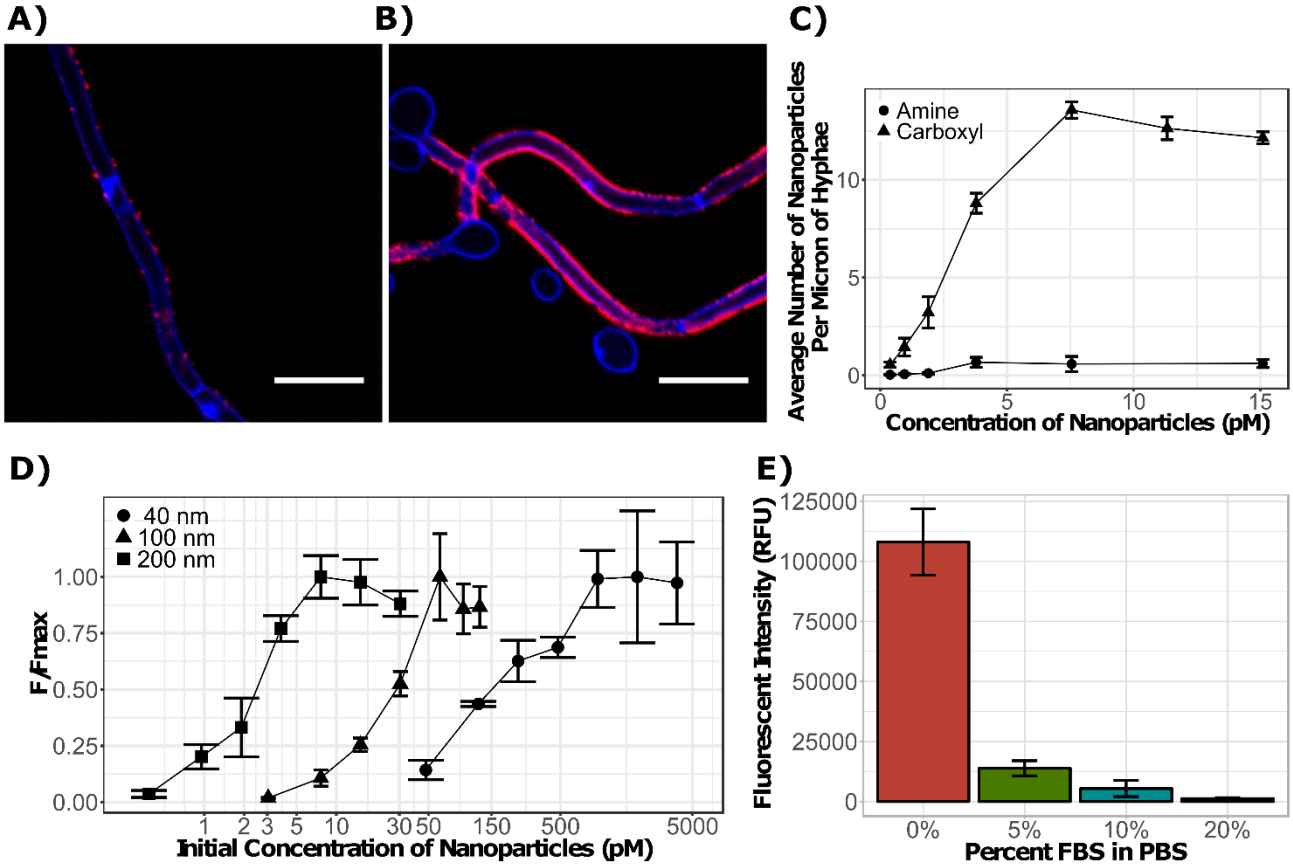


**C.** Binding profiles for 200 nm amine and carboxylate nanoparticles onto hyphae. For each cell, 10 measurements were taken along the hyphae and averaged. The data points and error bars represent the mean and standard deviation of 3 hyphae, respectively. **D.** Equilibrium adsorption profile for 40, 100, and 200 nm carboxylate nanoparticles on hyphae. For each cell, 10 measurements were taken along the hyphae and averaged. The data points and error bars represent the mean and standard deviation of 4 hyphae. $F/F_{max}$ represents the relative fluorescent intensity (RFU) along one micron of hyphae divided by the maximum mean fluorescent intensity along a micron of hyphae. **E.** Effect of % FBS in PBS on 40 nm carboxylate nanoparticle binding. For each cell, 10 measurements were taken along one micron of the hyphae and averaged. The data points and error bars represent the mean and standard deviation of at least 3 hyphae.

surface was reached. As shown in the adsorption profiles in Figure 5D, the carboxylate nanoparticle binding increased with concentration until saturation. Concentrations were chosen to be within the dynamic range of fluorescent intensity measurements while achieving saturation of the hyphal cell wall for downstream analysis of binding affinity. The nanoparticles and hyphae were maintained in a state of equilibrium during these measurements. For comparison among the nanoparticles of different diameters, which have different fluorescent properties, saturation was observed as the maximum mean fluorescent intensity ($F_{max}$) measured along a micron of hyphae for each nanoparticle diameter and all measurements of that diameter were divided by this intensity. The results show that larger nanoparticles have higher molar binding affinities.

For medical applications of detection and treatment, nanoparticle binding must take place in blood *in vivo* or in an isolated blood sample, which contain serum proteins. We therefore characterized the binding of carboxylate nanoparticles in PBS to hyphae grown in Spider medium for 3 hours with the addition of fetal bovine serum (FBS). Adding FBS decreases the binding of both 40 nm and 200 nm carboxylate nanoparticles to the surface of the hyphal cell wall (Supplementary Information Figure S2). As shown in Figure 5E, binding of 40 nm carboxylate nanoparticles is reduced at FBS concentrations ranging from 5 to 20% ($P<0.001$). A side effect of serum addition is aggregation – nanoparticle interaction occurs (Table 1) and larger yeast and hyphal aggregates form in PBS with increasing serum addition (data not shown).

**Nanoparticle surface charge and diameter influence nanoparticle adhesion**

We have observed that highly charged carboxyl-functionalized nanoparticles have a strong propensity to adsorb on *C. albicans* hyphae, unlike amine-functionalized nanoparticles in the same medium (Figure 5C), and the diameter of nanoparticles closely linked to the particle concentration at which the hyphae are saturated (Figure 5D). Langmuir was the first describe the reversible chemical binding of a reactant to equivalent binding sites on a uniform monolayer surface.[48] The advantage of Langmuir's theoretical framework is that it allows us to understand the adsorption behaviour using a simple model and estimate the binding energy of adsorption. The nanoparticle isotherms in this study illustrated Langmuir-like behaviour, in that the nanoparticles increase in binding with increasing concentrations, before saturating the cell wall.

In a system at equilibrium and with excess ligand to receptor, the concentration at which the surface of the hyphae is half saturated is roughly the dissociative binding constant ($K_D$), which an important parameter in the design of ligand-receptor systems.[49] From Figure 5D, we see that the dissociative

binding constant for the 40 nm nanoparticles was ~150pM, for 100 nm nanoparticles was ~30 pM and for 200 nm nanoparticles was ~2.5 pM. These are relatively small values of $K_D$ that scale like $(radius)^{-3/2}$ (linear regression, $R^2$=0.99995). In comparison, it has been shown that the N-terminus of Als1 binding to BSA-fucose, laminin, and fibronectin has a $K_D$ of ~21 mM, 130 mM, and 1.6 µM, respectively, values which are much higher and thus illustrate weaker binding.[50] This leads us to observe that nanoparticles formulations may be useful means to enhance drug delivery to *C. albicans*.

Langmuir's theory can be used to analyse the nature of the nanoparticle-cell interaction. The Gibbs free energy ($\Delta G$) of nanoparticle adsorption can be determined from the adsorption isotherms if we assume the adsorbed nanoparticles are in equilibrium with the nanoparticles in solution. Under these conditions the free energy of adsorption is a logarithmic function of $K_D$

$$\Delta G = RT ln(K_D) \quad (1)$$

where $R$ is the ideal gas law constant and $T$ is temperature. At room temperature $\Delta G$ was -55 kJ/mol for the 40 nm nanoparticles, -59 kJ/mol for the 100 nm nanoparticles, and -65 kJ/mol for the 200 nm nanoparticle, placing this interaction in a range between strong physiosorption and chemisorption, thus implying an ionic interaction. The energy of adsorption is equal to the product of the work of adhesion ($\gamma$) of the bead-hyphae interaction and area of contact. Work of adhesion is a function of interface material properties: the hyphal surface remains consistent under controlled experimental conditions, while the nanoparticles have the same core material, surface coating and shape. DLS measurements (Table 1) of nanoparticles in PBS showed insignificant differences in zeta potential values of the different diameter carboxylate particles. Thus, the $\Delta G$ differences seen here are mediated not by $\gamma$ but rather by changes in the contact area. As expected, the magnitude of the adsorption energy increased with particle diameter and it was observed that $K_D$ scales with the -3/2 power of the particle radius ($r$).

$$K_D \sim r^{-\frac{3}{2}} \quad (2)$$

This scaling behavior indicates that bead-hyphae contact area does not follow a simple contact mechanics model. For example, if the Johnson-Kendall-Roberts (JKR) model were valid we would expect $K_D$ to decrease exponentially with the 4/3 power of particle radius.[51]

$$K_D \sim e^{-r^{\frac{4}{3}}} \quad (3)$$

The weaker dependence of adsorption energies on particle radius for our experimental results compared to a JKR model could result from the nanometer scale roughness of the surface of the hyphae or changes in the mechanical properties of its membrane.

**Nanoparticles bind to Als3 protein of *C. albicans***

We have shown in this study that carboxylate nanoparticles of varying diameters bind preferentially to the hyphae of *C. albicans*. Amine nanoparticles of the same diameter did not bind to the hyphae, and the presence of serum in solution reduces nanoparticle adhesion. Using strains deficient in Als and Hwp protein production, we found that nanoparticle binding was closely linked to the presence of Als3. Als3 has been shown to be localized to the germ tube and hyphae, when grown in the same conditions used in this study.[38] When the *ALS3* gene is deleted, we saw reduced localization of the nanoparticles to hyphae, and increased localization around the neck of the germ tube, which is consistent with immunolabelling of Als1 and Als4[46,47] under the same growth conditions. This indicates that whereas Als3 is the preferential and strongest mediator of binding of nanoparticles, Als1 or Als4 may be secondary, weaker mediators of binding.

We also observed an increase in binding of nanoparticles to yeast phase cells in the Δals3 mutant. Als1 is expressed on yeast phase cells in populations placed in new growth media.[46] The increased binding of nanoparticles to yeast cells, in fresh media and in the absence of Als3 only, indicates that Als1 is a secondary binder. In the absence of Als3, carboxylate nanoparticles bind to Als1 on the neck of the germ tubes and on yeast cells.

*C. albicans* binds to a wide variety of ligands, and Als proteins have long been implicated in much of this adhesion. Magnetic beads of 0.7 µm in diameter coated in either BSA, fibronectin, type IV collagen, laminin and casein have been shown to bind to various *C. albicans* morphological forms, and to *Saccharomyces cerevisiae* expressing Als5.[52] As reviewed by Hoyer et al 2016, Als proteins have been shown to regulate binding to host tissue, initiate biofilm formation, and be responsible for binding to abiotic materials. Als3 in particular has been shown to be one of the strongest mediators of adhesion.[37,43] Deletion of *ALS3* has been shown to reduce binding of *C. albicans* by 42-63% to endothelial cells and 60% to buccal epithelial cells and deletion of *ALS1* has also been shown to reduce binding to endothelial cells by 20%.[28] Our results show that the deletion of *ALS3* reduced nanoparticle adhesion along the hyphae and increased localized binding to Als1, allowing us to add carboxylate nanoparticles of diameters from 40-200 nm to the growing list of ligands recognized by Als proteins. In addition, binding of the negatively-charged nanoparticles to the hyphae observed in our study was similar to the binding pattern of bacteria such as *S. aureus*[42] *Streptococcus gordonii*[41] and *Pseudomonas aeruginosa*[53] to *C. albicans*, which is interesting as bacteria have a net negative charge on the cell surface.[17]

Binding of nanoparticles to *C. albicans* is unlikely to be caused by hydrophobic interactions. Cell surface hydrophobicity of *C. albicans* cell surface varies under different growth conditions[24],and germ tubes and hyphae are more hydrophobic. [23,24] Als protein abundance has often been linked to cell surface hydrophobicity. However, the nanoparticles studied here are coated in a hydrophilic polymer containing carboxylic acid groups, and have a zeta potential that varies between -28 and -33 mV. This makes it unlikely that

hydrophobicity is the mediator of attachment to the hyphae. This is supported by the observation that *S. cerevisiae* displaying fusion surface proteins with Als regions bind to a variety of abiotic surfaces, such as polypropylene, borosilicate glass and polyvinylchloride, without any correlation to cell surface hydrophobicity.[37] These observations, combined with our analysis of the $\Delta G$ of the interaction being within the range of strong physiosorption, support the conclusion that *C. albicans* binding to abiotic nanoparticles is governed instead by ionic interactions mediated by Als proteins.

Als proteins have four domains: the N-terminal (NT) domain, the T-domain, a series of tandem repeats and the C-terminal domain.[54] The NT-domain is responsible for adhesion. Resolving the Als3 structure revealed that the NT-region of Als3 (amino acids 1-315) has a peptide binding cavity (PBC), which binds the carboxyl end of a flexible C-termini peptide of up to six amino acids by establishing a salt bridge between the negative C-termini and positive side chain amine in the PBC.[55,56] The NT-region also has a short conserved amyloid forming region (AFR), which has been shown to mediate interactions between Als proteins and cause aggregation among *C. albicans* cells.[57] The adhesive properties of Als3 have been attributed to the PBC – mutating the PBC results in the same reduction in adherence to human epithelial and endothelial cells as deleting the entire *ALS3* gene, whereas mutating the AFR has no effect on adhesion.[56] Binding to *S. gordonii* by Als3 is also mediated by the PBC only.[27] The ability of the PBC to form a salt bridge with a negatively charged ligand suggests that the positively charged lysine at the end of the PBC may mediate the interaction with carboxylate nanoparticles. However, the width of an amino acid is on the scale of one nanometer, and the nanoparticles in our study range from 40-200nm, with high-density carboxylic acids functionalized directly on the surface. This makes it unlikely the nanoparticle is entering the PBC as a peptide would, and thus we do not confirm this mechanism. Consequently, though our analysis allows us to deduce that the interaction is ionic, and mediated by Als proteins, the precise mechanism of the interaction is unknown.

#### Presence of serum reduces nanoparticle adhesion

The presence of serum is an important factor when considering nanoparticle interactions with fungi for *in vivo* applications, due to the high concentration of proteins which may adsorb to the nanoparticles.[58] From DLS measurements (Table 1), the reduction in zeta potential of the nanoparticles in the presence of serum suggests that the charge is masked by the adsorption of a protein layer on the nanoparticle. The adsorption of proteins has been shown to reduce nanoparticle adhesion and uptake.[11,58] The presence of denatured BSA (bovine serum albumin) and BSA immobilized on particles or surfaces has also been shown to induce aggregation in *C. albicans*[59,60] a phenomenon which will influence nanoparticle adhesion by competing with or blocking binding sites. Additionally, given the broad binding recognition of Als proteins, Als3 and Als1 may be binding to other serum proteins in the FBS. Our experiments cannot determine whether reduction of nanoparticle adhesion is due to charge masking of nanoparticle by serum proteins, ligand binding of Als3 with serum proteins, or increased aggregation among hyphal cells.

## Conclusions

In this study we present the first detailed examination of the interactions between *C. albicans* hyphae and carboxylate polystyrene nanoparticles. Carboxylate nanoparticles of varying diameter were shown to bind only to the hyphae and not yeast cells of *C. albicans*, and nanoparticles were shown to adhere to the cell wall of *C. albicans*. Extensive analysis of interactions with yeast cells, germ tubes and hyphae of mutant *C. albicans* strains deficient in key hyphal surface proteins showed that Als3 is the primary mediator, with Als1 possibly having a secondary role.

Carboxylate nanoparticles showed increase in binding with increase in concentration until the surface was saturated, a trend similar to a Langmuir model based on monolayer adsorption. Calculated dissociative binding constants ($K_D$) were on the scale of pM and placed the interaction in the ionic strength range. The addition of serum decreased binding of nanoparticles to the surface of *C. albicans*. Future scientific studies could analyse the force-distance behaviour of the interaction between Als3 and carboxylate nanoparticles and determine the exact molecular mechanism of interaction.

Nanoparticles have the potential to diagnose and treat *C. albicans* through adhesion to the hyphal cell wall. As previously stated, magnetic nanoparticles can be used for separation. We have shown that a 200 nm negatively-charged nanoparticle has high binding affinity for *C. albicans.* A 200nm magnetic nanoparticle, which would have high magnetic mobility compared to a 40 or 100 nm nanoparticle, could be used for cheap and effective separation of *C. albicans* for PCR or microscopy from a low-serum or diluted blood sample. Additionally, diagnostics and therapeutics could benefit from targeting the Als3 protein, which has a natural affinity for nanoparticles. The functionalization of a peptide with a high affinity for Als3 to a nanoparticle with minimal protein adsorption would be ideal. The T2Candida system has already demonstrated the use of superparamagnetic particles *in vitro* diagnostics, when used to detect of PCR products from *Candida* spp.[7] Here, we show that nanoparticles have alternative potential for diagnosis and treatment of bloodstream infections through hyphal cell wall adhesion. For example, magnetic nanoparticles could allow us to image and identify the area of infection *in vivo* using MRI and to extract *C. albicans* using magnetic separation techniques from a blood sample. Other nanoparticles paired with appropriate imaging techniques could be used to classify an infection as fungal or bacterial and to deliver anti-fungals directly to the site of infection.

## Acknowledgements

This program of research has been supported by the Whitaker International Program of the IEE and the Science Foundation of Ireland (08/IN1/B2072, 15/IA/3127, and 12/IA/1343). *Candida* strains were kindly provided by Professor Lois L Hoyer, Department of Pathobiology, University of Illinois at Urbana-Champaign, Urbana, IL, USA, Professor Aaron P. Mitchell, Department of Biological Sciences, Carnegie Mellon University, Pittsburgh, PA, USA, and Dr Selene Mogavero, Department of Microbial Pathogenicity Mechanisms, Hans Knöll Institute, D-07745 Jena, Germany.

## References

1 M. A. Pfaller and M. Castanheira, *Med. Mycol.*, 2015, **54**, myv076.

2 P. G. Pappas, C. A. Kauffman, D. R. Andes, C. J. Clancy, K. A. Marr, L. Ostrosky-Zeichner, A. C. Reboli, M. G. Schuster, J. A. Vazquez, T. J. Walsh, T. E. Zaoutis and J. D. Sobel, *Clin. Infect. Dis.*, 2016, **62**, e1-50.

3 L. Drgona, A. Khachatryan, J. Stephens, C. Charbonneau, M. Kantecki, S. Haider and R. Barnes, *Eur. J. Clin. Microbiol. Infect. Dis.*, 2014, **33**, 7–21.

4 M. J. S. Mendes Giannini, T. Bernardi, L. Scorzoni, A. M. Fusco-Almeida and J. C. O. Sardi, *J. Med. Microbiol.*, 2013, **62**, 10–24.

5 T. Avni, L. Leibovici and M. Paul, *J. Clin. Microbiol.*, 2011, **49**, 665–70.

6 G. Marklein, M. Josten, U. Klanke, E. Müller, R. Horré, T. Maier, T. Wenzel, M. Kostrzewa, G. Bierbaum, A. Hoerauf and H.-G. Sahl, *J. Clin. Microbiol.*, 2009, **47**, 2912–7.

7 E. Mylonakis, C. J. Clancy, L. Ostrosky-Zeichner, K. W. Garey, G. J. Alangaden, J. A. Vazquez, J. S. Groeger, M. A. Judson, Y.-M. Vinagre, S. O. Heard, F. N. Zervou, I. M. Zacharioudakis, D. P. Kontoyiannis and P. G. Pappas, *Clin. Infect. Dis.*, 2015, **60**, 892–899.

8 M. D. LaFleur, C. A. Kumamoto and K. Lewis, *Antimicrob. Agents Chemother.*, 2006, **50**, 3839–3846.

9 A. Neuwelt, N. Sidhu, C.-A. A. Hu, G. Mlady, S. C. Eberhardt and L. O. Sillerud, *Am. J. Roentgenol.*, 2015, **204**, W302–W313.

10 C. M. Beddoes, C. P. Case and W. H. Briscoe, *Adv. Colloid Interface Sci.*, 2015, **218**, 48–68.

11 A. Lesniak, F. Fenaroli, M. P. Monopoli, C. Åberg, K. A. Dawson and A. Salvati, *ACS Nano*, 2012, **6**, 5845–5857.

12 I. Sondi and B. Salopek-Sondi, *J. Colloid Interface Sci.*, 2004, **275**, 177–182.

13 S. Pal, Y. K. Tak and J. M. Song, *Appl. Environ. Microbiol.*, 2007, **73**, 1712–1720.

14 Z. V. Feng, I. L. Gunsolus, T. A. Qiu, K. R. Hurley, L. H. Nyberg, H. Frew, K. P. Johnson, A. M. Vartanian, L. M. Jacob, S. E. Lohse, M. D. Torelli, R. J. Hamers, C. J. Murphy, C. L. Haynes, Y. Su, M. Yang, D. L. Kaplan, M. R. Zakin, M. J. Slepian, Y. Huang, F. G. Omenetto and J. A. Rogers, *Chem. Sci.*, 2015, **6**, 5186–5196.

15 C. M. Goodman, C. D. Mccusker, T. Yilmaz and V. M. Rotello, *Bioconjug. Chem.*, 2004, **15**, 897–900.

16 J. Kim and P. Sudbery, *J. Microbiol.*, 2011, **49**, 171–177.

17 A. Brown, Lisa, Wolf, Julie M., Prados-Rosales, Rafael, Casadevall, *Nat. Rev. Microbiol.*, 2015, **Volume 13**, 620–630.

18 P. Uppuluri and J. L. Lopez-Ribot, *PLoS Pathog.*, 2016, **12**, e1005397.

19 H. H. Lara, D. G. Romero-Urbina, C. Pierce, J. L. Lopez-Ribot, M. J. Arellano-Jiménez and M. Jose-Yacaman, *J. Nanobiotechnology*, 2015, **13**, 91.

20 K. Niemirowicz, B. Durnaś, G. Tokajuk, K. Głuszek, A. Z. Wilczewska, I. Misztalewska, J. Mystkowska, G. Michalak, A. Sodo, M. Wątek, B. Kiziewicz, S. Góźdź, S. Głuszek and R. Bucki, *Nanomedicine Nanotechnology, Biol. Med.*, 2016, **12**, 2395–2404.

21 B. M. Geilich, I. Gelfat, S. Sridhar, A. L. van de Ven and T. J. Webster, *Biomaterials*, 2017, **119**, 78–85.

22 P. Sudbery, N. Gow and J. Berman, *Trends Microbiol.*, 2004, **12**, 317–324.

23 A. Beaussart, D. Alsteens, S. El-Kirat-Chatel, P. N. Lipke, S. Kucharíková, P. Van Dijck and Y. F. Dufrêne, *ACS Nano*, 2012, **6**, 10950–64.

24 B. W. Hazen and K. C. Hazen, *Infect. Immun.*, 1988, **56**, 2521–5.

25 A. Lesniak, A. Campbell, M. P. Monopoli, I. Lynch, A. Salvati and K. A. Dawson, *Biomaterials*, 2010, **31**, 9511–9518.

26 A. Panarella, M. G. Bexiga, G. Galea, E. D. O 'Neill, A. Salvati, K. A. Dawson and J. C. Simpson, *Sci. Rep.*, 2016, **6**, 28865.

27 L. L. Hoyer, S.-H. Oh, R. Jones and E. Cota, *Front. Microbiol.*, 2014, **5**, 564.

28 X. Zhao, S.-H. Oh, G. Cheng, C. B. Green, J. A. Nuessen, K. Yeater, R. P. Leng, A. J. P. Brown and L. L. Hoyer, *Microbiology*, 2004, **150**, 2415–2428.

29 A. M. Gillum, E. Y. Tsay and D. R. Kirsch, *Mol. Gen. Genet.*, 1984, **198**, 179–82.

30 A. Porta, A. M. Ramon and W. A. Fonzi, *J. Bacteriol.*, 1999, **181**, 7516–23.

31 M. M. Harriott and M. C. Noverr, *Antimicrob. Agents Chemother.*, 2010, **54**, 3746–55.

32 X. Zhao, S.-H. Oh, K. M. Yeater and L. L. Hoyer, *Microbiology*, 2005, **151**, 1619–30.

33 A. A. Sanchez, D. A. Johnston, C. Myers, J. E. Edwards, A. P. Mitchell, S. G. Filler and S. G. Filler, *Infect. Immun.*, 2004, **72**, 598–601.

34 P. Sundstrom, J. E. Cutler and J. F. Staab, *Infect. Immun.*, 2002, **70**, 3281–3.

35 D. Hopwood, E. M. Spiers, P. E. Ross, J. T. Anderson, J. B. McCullough and F. E. Murray, *Gut*, 1995, **37**, 598–602.

36 T. Nomura, Y. Kuriyama, H. Tokumoto and Y. Konishi, *J. Nanoparticle Res.*, 2015, **17**, 105.

37 W. Aoki, N. Kitahara, N. Miura, H. Morisaka, K. Kuroda and M. Ueda, *FEMS Immunol. Med. Microbiol.*, 2012, **65**, 121–124.

38 D. A. Coleman, S.-H. Oh, X. Zhao, H. Zhao, J. T. Hutchins, J. H. Vernachio, J. M. Patti and L. L. Hoyer, *J. Microbiol. Methods*, 2009, **78**, 71–8.

39 Q. T. Phan, C. L. Myers, Y. Fu, D. C. Sheppard, M. R. Yeaman, W. H. Welch, A. S. Ibrahim, J. E. Edwards and S. G.

Filler, *PLoS Biol.*, 2007, **5**, e64.
40 S. Tati, P. Davidow, A. McCall, E. Hwang-Wong, I. G. Rojas, B. Cormack and M. Edgerton, *PLoS Pathog.*, 2016, **12**, e1005522.
41 R. J. Silverman, A. H. Nobbs, M. M. Vickerman, M. E. Barbour and H. F. Jenkinson, *Infect. Immun.*, 2010, **78**, 4644–4652.
42 B. M. Peters, E. S. Ovchinnikova, B. P. Krom, L. M. Schlecht, H. Zhou, L. L. Hoyer, H. J. Busscher, H. C. van der Mei, M. A. Jabra-Rizk and M. E. Shirtliff, *Microbiology*, 2012, **158**, 2975–86.
43 C. V Bamford, A. H. Nobbs, M. E. Barbour, R. J. Lamont and H. F. Jenkinson, *Microbiology*, 2015, **161**, 18–29.
44 J. F. Staab, S. D. Bradway, P. L. Fidel and P. Sundstrom, .
45 C. J. Nobile, J. E. Nett, D. R. Andes and A. P. Mitchell, *Eukaryot. Cell*, 2006, **5**, 1604–10.
46 D. A. Coleman, S.-H. Oh, X. Zhao and L. L. Hoyer, *Microbiology*, 2010, **156**, 3645–59.
47 D. A. Coleman, S.-H. Oh, S. L. Manfra-Maretta and L. L. Hoyer, *FEMS Immunol. Med. Microbiol.*, 2012, **64**, 321–33.
48 I. Langmuir, *J. Am. Chem. Soc.*, 1917, **39**, 1848–1906.
49 T. D. Pollard, *Mol. Biol. Cell*, 2010, **21**, 4061–7.
50 D. S. Donohue, F. S. Ielasi, K. V. Y. Goossens and R. G. Willaert, *Mol. Microbiol.*, 2011, **80**, 1667–1679.
51 K. L. Johnson, K. Kendall and A. D. Roberts, *Proc. R. Soc. London A Math. Phys. Eng. Sci.*
52 N. K. Gaur, R. L. Smith and S. A. Klotz, *Cell Commun. Adhes.*, **9**, 45–57.
53 D. A. Hogan and R. Kolter, *Science*, 2002, **296**, 2229–32.
54 L. L. Hoyer and E. Cota, *Front. Microbiol.*, 2016, **7**, 280.
55 P. S. Salgado, R. Yan, J. D. Taylor, L. Burchell, R. Jones, L. L. Hoyer, S. J. Matthews, P. J. Simpson and E. Cota, *Proc. Natl. Acad. Sci. U. S. A.*, 2011, **108**, 15775–9.
56 J. Lin, S. H. Oh, R. Jones, J. A. Garnett, P. S. Salgado, S. Rusnakova, S. J. Matthews, L. L. Hoyer and E. Cota, *J. Biol. Chem.*, 2014, **289**, 18401–18412.
57 P. N. Lipke, C. Ramsook, M. C. Garcia-Sherman, D. N. Jackson, C. X. J. Chan, M. Bois and S. A. Klotz, *New J. Sci.*, 2014, **2014**, 815102.
58 S. Ritz, S. Schöttler, N. Kotman, G. Baier, A. Musyanovych, J. Kuharev, K. Landfester, H. Schild, O. Jahn, S. Tenzer and V. Mailänder, *Biomacromolecules*, 2015, **16**, 1311–1321.
59 S. A. Klotz, N. K. Gaur, D. F. Lake, V. Chan, J. Rauceo and P. N. Lipke, *Infect. Immun.*, 2004, **72**, 2029–34.
60 S. P. Hawser and K. Islam, *Infect. Immun.*, 1998, **66**, 140–4.